AGU PUBLICATIONS

JGR

Journal of Geophysical Research: Space Physics

RESEARCH ARTICLE
10.1002/2016JA022462

Special Section:
Energetic Electron Loss and its Impacts on the Atmosphere

BARREL observations of a solar energetic electron and solar energetic proton event

A. J. Halford[1,2], S. L. McGregor[3], M. K. Hudson[1], R. M. Millan[1], and B. T. Kress[4]

[1]Department of Physics and Astronomy, Dartmouth College, Hanover, New Hampshire, USA, [2]Goddard Space Flight Center, NASA, Greenbelt, Maryland, USA, [3]Department of Physics, Keene State College, Keene, New Hampshire, USA, [4]NOAA, Boulder, Colorado, USA

Key Points:
- The precipitation of solar energetic proton events can be observed and studied by BARREL
- BARREL is able to observe the precipitation of solar energetic electron events on open field lines
- Using observations of solar energetic electrons allows for mapping of the open-closed boundary

Correspondence to:
A. J. Halford,
Alexa.J.Halford@Dartmouth.edu

Citation:
Halford, A. J., S. L. McGregor, M. K. Hudson, R. M. Millan, and B. T. Kress (2016), BARREL observations of a solar energetic electron and solar energetic proton event, *J. Geophys. Res. Space Physics*, *121*, 4205–4216, doi:10.1002/2016JA022462.

Received 29 JAN 2016
Accepted 30 MAR 2016
Accepted article online 4 APR 2016
Published online 12 MAY 2016

Abstract During the second Balloon Array for Radiation Belt Relativistic Electron Losses (BARREL) campaign two solar energetic proton (SEP) events were observed. Although BARREL was designed to observe X-rays created during electron precipitation events, it is sensitive to X-rays from other sources. The gamma lines produced when energetic protons hit the upper atmosphere are used in this paper to study SEP events. During the second SEP event starting on 7 January 2014 and lasting ~3 days, which also had a solar energetic electron (SEE) event occurring simultaneously, BARREL had six payloads afloat spanning all magnetic local time (MLT) sectors and L values. Three payloads were in a tight array (~2 h in MLT and ~2 ΔL) inside the inner magnetosphere and at times conjugate in both L and MLT with the Van Allen Probes (approximately once per day). The other three payloads mapped to higher L values with one payload on open field lines for the entire event, while the other two appear to be crossing from open to closed field lines. Using the observations of the SEE and SEP events, we are able to map the open-closed boundary. Halford et al. (2015) demonstrated how BARREL can monitor electron precipitation following an interplanetary shock created by a coronal mass ejection (ICME-shock) arrival at Earth, while in this study we look at the SEP event precursor to the arrival of the ICME-Shock in our cradle-to-grave view: from flare, to SEE and SEP events, to radiation belt electron precipitation.

1. Introduction

Since the 1940s, solar energetic particle events have been studied by balloons [e.g., *Bazilevskaya et al.*, 2010; *Velinov et al.*, 2013; *Woodger et al.*, 2015], ground-based [e.g., *Forbush*, 1946; *LaBelle*, 2004; *Miroshnichenko et al.*, 2013; *Rogers and Honary*, 2015], and in situ measurements [*Kahler*, 2001; *Kühl et al.*, 2015; *Adriani et al.*, 2015; *Gershman et al.*, 2015], as well as through modeling [e.g., *Kress et al.*, 2008, 2010; *Kozarev et al.*, 2013]. Between 6 and 10 January 2014 there were two solar energetic proton (SEP) events [e.g., *Kühl et al.*, 2015; *Möstl et al.*, 2015]. Both events have been of great interest to the heliospheric community [e.g., *Savani et al.*, 2015; *Mays et al.*, 2015; *Möstl et al.*, 2015; *Kühl et al.*, 2015; *Halford et al.*, 2015]. At this time an array of payloads from the Balloon Array for Radiation belt Relativistic Electron Losses (BARREL) mission of opportunity were afloat, five for the first and six for the second SEP event, Figure 1. The first of these SEP events occurred on 6 January 2015. The second SEP event was part of a Sun-to-mud study by *Halford et al.* [2015] that focused on how the solar storm ultimately led to the loss of electrons from the radiation belts despite not producing a significant geomagnetic storm, where $Kp < 4$ during the entire 4 days. In terms of electron radiation belt dynamics, it took approximately 2.5 days from the release of energy at the Sun to affect the outer zone electrons. However, from about 40 min after the observation of the X-class flare (~18:00 UT on 7 January 2014), and continuing throughout the better part of the next 3 days, the Earth's atmosphere was awash with solar energetic particles. With the array of balloons as well as in situ measurements from GOES, ACE, and the Van Allen Probes, we are able to study how the solar energetic proton event propagated through the magnetosphere and was lost to the atmosphere.

Solar energetic electron (SEE) events are found to sometimes accompany SEP events [*Mewaldt et al.*, 2005], and both of their sources can be distinguished by their temporal properties. SEP events are subdivided into impulsive and gradual events, the former corresponding to acceleration at the reconnection site at the Sun and the latter to acceleration by the interplanetary shock created by a coronal mass ejection (ICME-shock) as it propagates earthward [*Reames*, 1999]. SEE events are thought to be generated at and due to the mechanics

Figure 1. A map of the flight paths for the six BARREL payloads up during the SEE and SEP events from 7 January 00:00 UT to 10 January 00:00 UT.

and aftermath of the solar flare [e.g., *Reames*, 1999; *Kontar and Reid*, 2009] but may also be associated with acceleration of electrons through the shock region similar to the processes generating the SEP events [e.g., *Reames*, 1999; *Klassen et al.*, 2002]. As the event that we will consider lasts for multiple days, it is likely that at least a portion of the SEE event is associated with the acceleration through the ICME-shock. However,

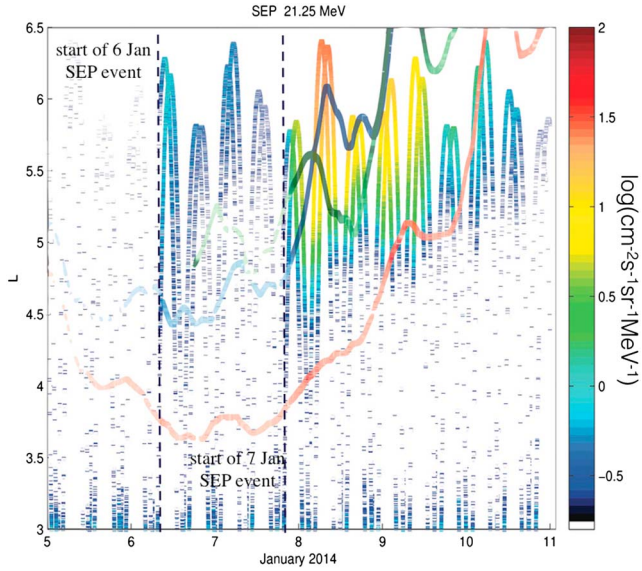

Figure 2. SEP events observed by the REPT instruments on Van Allen probes A and B for the energy channel centered around 21.25 MeV. The *y* axis is McIlwain *L* value [*McIlwain*, 1966] (using International Geomagnetic Reference Field plus OP77Q in which REPT Level 3 flux data are plotted), *x* axis is time, and the color represents the log of the flux of the protons. Overlaid are the proton proxies from the BARREL payloads 2K (blue), 2L (green), and 2X (red) where their intensity represents the counts of X-rays observed in the proton proxies to give a qualitative comparison of SEP event flux intensity at BARREL to compare with REPT, also mapped spatially in *L*.

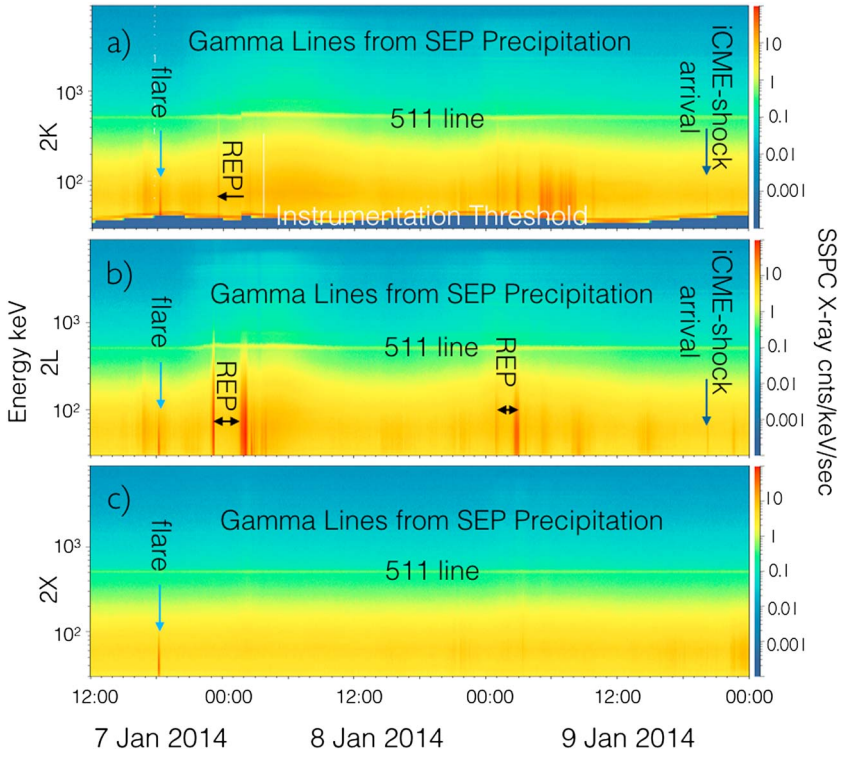

Figure 3. The slow spectra (SSPC) data, 32 s integration, and 256 energy channels, for the three payloads which mapped to the inner magnetosphere, (a) 2K, (b) 2L, and (c) 2X. The X-ray event due to the X-class flare which was part of the solar storm producing the SEP event is highlighted with the blue arrow. The X-ray increases due to precipitation of relativistic electrons (black arrows) and the electron loss observed when the ICME-shock hit the magnetosphere and discussed in *Halford et al.* [2015] are also highlighted (dark blue arrow). The 511 line which is used for energy calibration is labeled as is the region where the gamma lines from the SEP precipitation can be seen (above 500 keV).

we will not try to decipher which mechanism causes the generation of either the SEE or SEP event in this paper but instead use the existence of the SEE event in order to consider mapping the boundary between open and closed field lines at the Earth's magnetosphere.

The SEP event on 6 January 2014, which was classified as a ground level enhancement as well as being observed at Mars, has been well documented in previous work [*Kühl et al.*, 2015, and references therein]. Although the Van Allen Probes observed the protons entering into the inner magnetosphere on 6 January 2014, as well as BARREL observing their loss, the event on 7 January 2014 had a much higher flux of lower energy (1 to 10s of MeV) protons observed both at Van Allen Probes and the BARREL balloons. This is likely due to the flux and characteristic energies associated with the event itself. Specifically, as seen in Figure 2, the flux of protons observed by the Relativistic Electron Proton Telescope (REPT) [*Baker et al.*, 2012] at the lower SEP event energies, ~20 MeV, is much higher for the second event. Thus, for this paper we will focus our results on the second of the two SEP events.

The 7 January 2014 event provides a unique set of observations. Although BARREL, which sits within the Earth's atmosphere at heights ranging from approximately 22–38 km, was designed to infer radiation belt electron loss, it can remotely observe the loss of SEP events in the atmosphere by observing gamma lines associated with the collision of protons with atmospheric neutrals as can be seen in Figures 3 and 4. During this event, BARREL had three payloads which mapped to the inner magnetosphere (Figure 3) and had conjunctions with the Van Allen Probes in both *L* and magnetic local time (MLT) at least once per day. The other three BARREL payloads aloft at this time were at higher latitudes. Payload 2I was on open field lines throughout the entire event period, while payloads 2T and 2W were moving between open and closed field lines throughout the event. When the payloads were on open field lines, they were able to infer the solar energetic electrons which are otherwise shielded out by the Earth's magnetosphere. In this paper we will show how this unique event and set of observations allows us to observe the open-closed boundary. Better mapping and understanding of the open-closed boundary has implications for a wide range of space physics

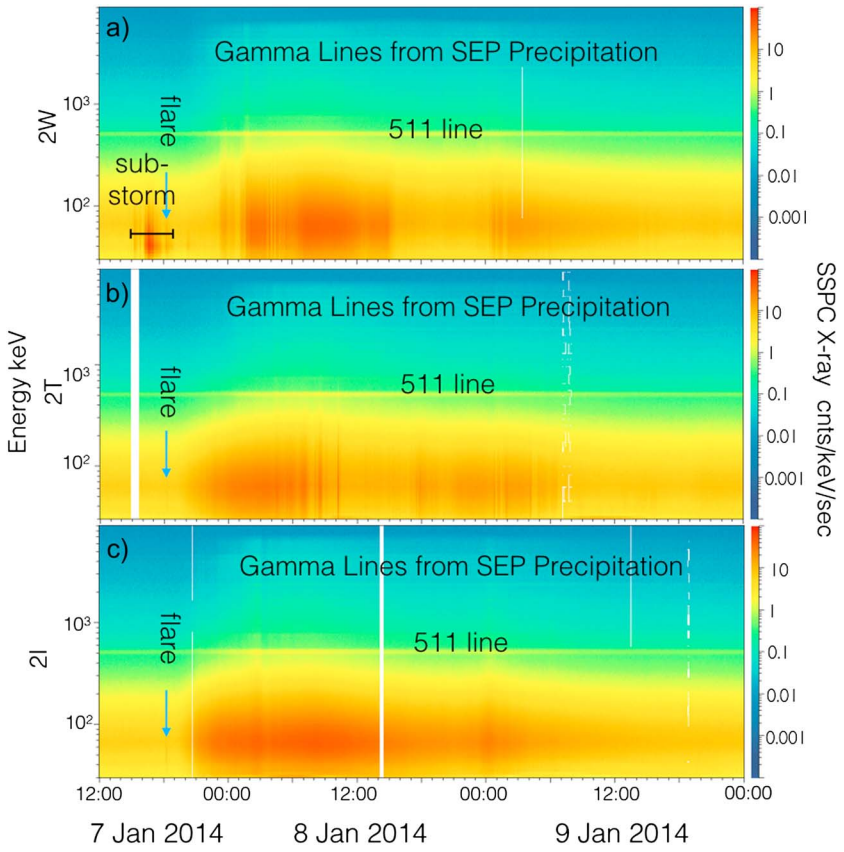

Figure 4. The SSPC data for the three payloads which mapped to the outer magnetosphere and open field lines, (a) 2W, (b) 2T, and (c) 2I. The X-ray event due to the X-class flare which was part of the solar storm producing the SEP event is highlighted with the blue arrows. The period of time where 2W infers radiation belt electron loss due to substorm dynamics is labeled. The solar flare occurs during the end of the precipitation event associated with the substorm. The 511 line is also highlighted which is used for energy calibration and is also noted as is the region where the gamma lines can be found.

topics. Determining the size and the rate of change of the boundary helps estimate the amount of energy being transferred from the Sun into our magnetosphere [e.g., *Rae et al.*, 2004; *Milan et al.*, 2012]. This can have implications for understanding not only the dynamics of magnetosphere-ionosphere coupling but also the cycle of storms and substorms which ultimately affects radiation belt dynamics.

2. Instrumentation and Methodology

The BARREL campaign launched a total of 20 balloons from two Antarctic stations, SANAE IV and Halley VI, during its second campaign from 27 December 2013 to 11 February 2014. The primary measurement objective was to observe X-rays produced by bremsstrahlung interactions of 10s keV - 10s MeV radiation belt electrons with the neutral atmosphere using a NaI spectrometer on each payload [*Millan et al.*, 2013]. The spectrometer is also sensitive to other sources of hard X-rays such as solar and cosmic gamma rays, gamma rays produced by deenergization and spallation from SEP events interacting with atmospheric neutrals, and 10s MeV protons producing X-rays as well as directly impacting the detector, all of which allow BARREL to observe gamma ray bursts, solar impulsive flares, and SEP events [*Woodger et al.*, 2015]. For this study we use the slow spectra (SSPC) which has 256 X-ray energy channels between ~30 keV and 10 MeV with a temporal resolution of 32 s.

When protons interact with the atmospheric neutral particles through spallation and deenergization, narrow gamma lines are produced [e.g., *Share and Murphy*, 2001], as can be seen in Figure 5, unlike the broad energy X-ray response from the bremsstrahlung process due to electron precipitation. We can use this observation to our advantage. As there were few observable electron precipitation events that extended into multiple MeV energy channels, the counts in the gamma lines above the 511 keV electron-positron annihilation line will

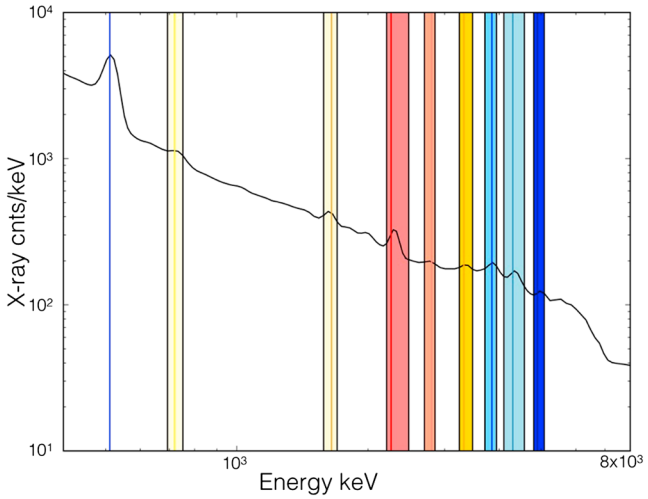

Figure 5. A slice in time of the SSPC data showing the energy spectra observed by payload 2T. The gamma lines are highlighted with straight lines. The shaded energy bins are summed together to create the proton proxy which is an array representing the loss of the SEP event to the atmosphere.

be dominated by the proton effects. By summing the energy bins associated with the narrow gamma lines produced by proton interactions in the atmosphere, we are able to construct a proxy showing the temporal structure of the precipitating solar protons at the location of the balloons. This new data product will be referred to as the proton proxy.

As stated above, the greater than tens of keV electrons lost to the atmosphere go through bremsstrahlung interactions producing a broad energy response in the X-ray detector. Thus, although we do not know the characteristic energy of the SEE event, or the shape of the associated energy spectrum, we can generate a proxy for the temporal electron response by summing the energy channels below 500 keV. This new data product will be referred to as the electron proxy. It should be noted that this alone will not distinguish between solar and radiation belt electrons. Both populations will produce the same response in the spectrometer. This type of analysis will also not provide energy information, but it does allow us to effectively differentiate between the electron and proton responses over long durations.

As during this time the detector was contaminated by the solar energetic protons, the publicly available GEANT response matrices for BARREL and the BARREL spectral analysis software (bdas) are unable to provide reliable predictions of the precipitating electron energy spectra. We are currently working on producing a similar GEANT modeling simulation as described in *Woodger et al.* [2015] to determine the response of the detector to the precipitating solar energetic protons. This should allow us to determine an energy spectrum of both the precipitating MeV protons and 10s keV to 10 MeV electrons. We also hope to eventually be able to provide information on the flux of the precipitation events similar to the analysis described in *Breneman et al.* [2015], but this is also left for future work as the GEANT response matrices are necessary for this approach. For now, by comparing the summed gamma lines with in situ observations, we are able to verify that BARREL saw loss of solar energetic electrons and protons to the atmosphere as well as start to narrow down the energy range of these particles through qualitative comparisons with ACE, GOES, and multiple energy channels of REPT (not shown here).

The NOAA Geostationary Operational Environmental Satellites (GOES) [*Singer et al.*, 1996] are a series of geosynchronous spacecraft which have become the primary source for real-time solar energetic particle data. Currently, the two operational GOES satellites are GOES 13 and 15. For the duration of the event, GOES 13 and 15 are located at a geographic latitude near 0° and longitudes of approximately 75°W and 135°W, respectively, in close conjunction in geomagnetic longitude with the Van Allen Probes and the three BARREL payloads which map to the inner magnetosphere. We use the Energetic Proton Electron and Alpha Detector (EPEAD) instrument as part of the Energetic Particle Sensors (EPS) which are on board the GOES satellites. EPEAD looks at proton energies ranging from 0.7 to 900 MeV. There are two EPEADs on each satellite, one looking east and one looking west. The 5 min averaged proton flux from the west viewing EPEAD on board GOES 15 is shown in Figure 6 (top) to give an overall picture of the solar proton fluxes for the January SEP event.

In order to look at the SEE event, we use the Advanced Composition Explore (ACE) satellites Electron, Proton, and Alpha Monitor (EPAM) suite of instruments. EPAM is a suite of five telescopes designed to look at high-energy electrons and protons. In particular, we focus on the Low Energy Foil Spectrometer (LEFS60)

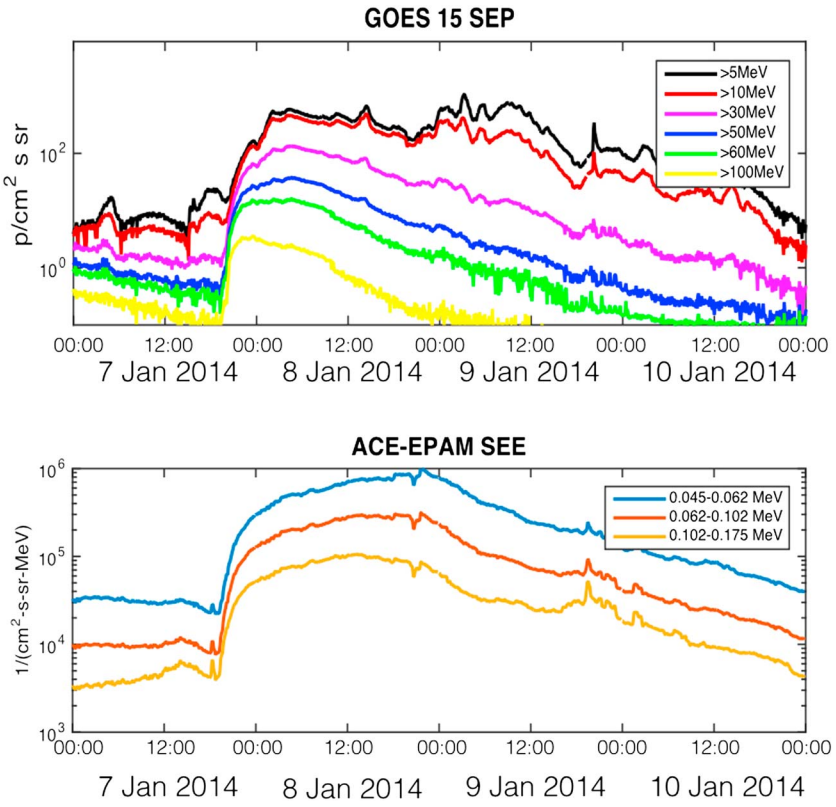

Figure 6. (top) Summed SEP event fluxes as measured by the EPEAD on board the GOES 15 spacecraft at 5 min resolution summed over different energy ranges for the time period starting on 7 January 2014 until 11 January 2014. (bottom) SEE event fluxes in the SW measured by the ACE EPAM instrument over the same time period.

telescope which measures ions and electrons above 35 keV at 60° to the satellite spin axis [*Gold et al.*, 1998]. We focus on the three available electron energy channels ranging from 45 to 175 keV which are shown in Figure 6 (bottom).

The Van Allen Probes are a pair of twin satellites in elliptical orbits with their perigee at approximately $L = 1.1$ and apogee at $L = 6.4$. During this event time period the apogee was within the noon-dusk sector. We use the data from the Relativistic Electron Proton Telescope (REPT), one of three instruments on the Energetic Particle, Composition, and Thermal Plasma (ECT) suite [*Spence et al.*, 2013]. The REPT instrument covers the proton energy range of 17–200 MeV to capture both radiation belt protons and those of solar origin. The solid-state detectors are directed perpendicular to the spin axis [*Baker et al.*, 2012]. For this paper we will be using the spin-averaged proton measurements.

3. Observations of the 7 January 2014 SEP Event: GOES and ACE Measurements

The Earth's magnetosphere was bombarded with solar energetic particles starting ~40 min after the observation of the X-class flare (~18:00 UT on 7 January 2014) and continuing throughout the better part of the next 3 days. Figure 6 (top) shows the SEP event observed by the GOES 15 spacecraft for the event starting on 7 January, while Figure 6 (bottom) shows the SEE event observed by the ACE-EPAM LEFS60 instrument. Both populations of energetic electrons and protons were already enhanced from their background levels due to the previous SEP event arrival on 6 January 2014. However, the rise in both energetic electrons and protons late on 7 January is clearly visible. The general profiles of the electrons and the protons differ, which is not unexpected as the protons and the electrons likely have different sources. For example, the flux of higher-energy solar protons start to decay prior to the electron peak which occurs later on 8 January. However, the lower energy protons (1–20 MeV) take the longest to recover staying at elevated levels throughout most of 9 January. For both the solar energetic proton and solar energetic electron events it took multiple days to recover to pre-event values.

4. SEP Events in the Inner Magnetosphere: Verification of Gamma Line Observations

As mentioned above we can consider separately the BARREL payloads that mapped to the inner magnetosphere and those that mapped to the outer magnetosphere during the SEP event of 7–10 January (Figure 1). First, we will focus on the three inner magnetospheric payloads to confirm that the increase in the proton proxy qualitatively matches observations of the SEP event in the inner magnetosphere at the Van Allen Probes. This approach will allow us to validate the usage of the summed gamma lines as a proton proxy for the SEP events when inferring the magnetic mapping to open or closed field lines in the following section.

The slow spectra for these three payloads can be seen in Figure 3. It is important to note that magnetospheric electron loss events can be observed throughout this time period: specifically, relativistic electron precipitation (REP) events in the evening of 7 January and ending on 8 January, as well as the loss of <500 keV radiation belt electron precipitation associated with substorm dynamics on 7 and 9 January 2014, the arrival of the ICME-shock on 8 January 2014 from the previous solar storm event discussed in *Thakur et al.* [2014], and the arrival of the ICME-shock on 9 January 2014 discussed in *Halford et al.* [2015]. The REP events often produce X-rays >511 keV and thus can be a source of contamination for the new proton proxy. As an example, during the REP event at ~23 UT on 7 January, the proton proxies of payloads 2K and 2L do see a short, sharp increase in flux, Figure 7 (a and b panels). This potential contamination is very dependent upon the characteristic energy and total flux of each individual REP event. For instance, during the REP event observed on 9 January at ~2:45 UT, an increase is not observed in the proton proxy as can be seen in Figure 7. Thus, the short-duration X-ray events produced by the loss of relativistic electrons to the atmosphere can be a source of contamination, but for the duration of the SEP events, the proton response dominates the proton proxy. Along the top of the panels are a set of horizontal lines corresponding to the *L* value as determined by the TS89 magnetic field model for $Kp = 6$ (red) and $Kp = 2$ (blue) [*Tsyganenko*, 1989]. In addition, the bar along the bottom of each panel in Figure 7 shows the magnetic local time where white is local noon and black is local midnight. What looks like a clear diurnal dependence of the normalized counts can be observed but may also be due to the temporal evolution of the SEP event. *Rogers and Honary* [2015] also observed a similar diurnal variation in riometer observations of SEP events. The most notable difference between the proton proxies of the three payloads is seen when comparing 2X with 2L and 2K. For all three payloads the counts begin to rise late on 7 January and have two peaks throughout the event, the first on 8 January and a second peak early on 9 January. Payloads 2L and 2K show larger overall counts in the proton proxy during the first peak on 8 January, which is nearly twice as large as the second peak. For payload 2X, this second peak on 9 January has a slightly larger count value than the first peak.

Throughout this event, the Van Allen Probes were traveling through the inner magnetosphere with their apogee in the noon-dusk sector. Figure 2 shows the log of the proton flux observed in REPT's proton energy channel centered around 21.5 MeV, the energy channel that the structure in the proton proxy most closely matches by eye. A direct comparison of the BARERL observations with the Van Allen Probes, which has an apogee at this time in the noon-dusk sector, is only possible when they are in the same MLT sector as the counts gathered by the balloon payloads are potentially affected by their local time location [e.g., *Rogers and Honary*, 2015]. The Earth's magnetosphere inhibits the penetration of these protons to reach a particular magnetospheric location (the cutoff rigidity). In general, the amount of geomagnetic shielding is inversely proportional to *L* leading to lower solar energetic proton fluxes at lower *L* values and higher fluxes at higher *L* values [e.g., *Kress et al.*, 2010; *Leske et al.*, 2001]. As the Van Allen Probes moved across *L* values, they were able to observe how far earthward the SEP event penetrated the magnetosphere.

Over-plotted on the REPT data are three lines depicting the mapped *L* value of three BARREL payloads 2K, 2L, and 2X that map to *L* values in the inner magnetosphere where the geomagnetic shielding of the SEP events is greater. An increase in opacity of the BARREL lines correspond to an increase in the proton proxy from Figure 7. Figure 2 shows that the BARREL payloads inferred similar increases and decreases of the SEP event precipitation when they were conjugate in *L* with the Van Allen Probes. The BARREL payloads 2K and 2L were at high enough *L* values to see proton precipitation throughout most of the SEP event. Payload 2X only saw increases from the background once it reached the *L* values where the SEP event was observed in situ.

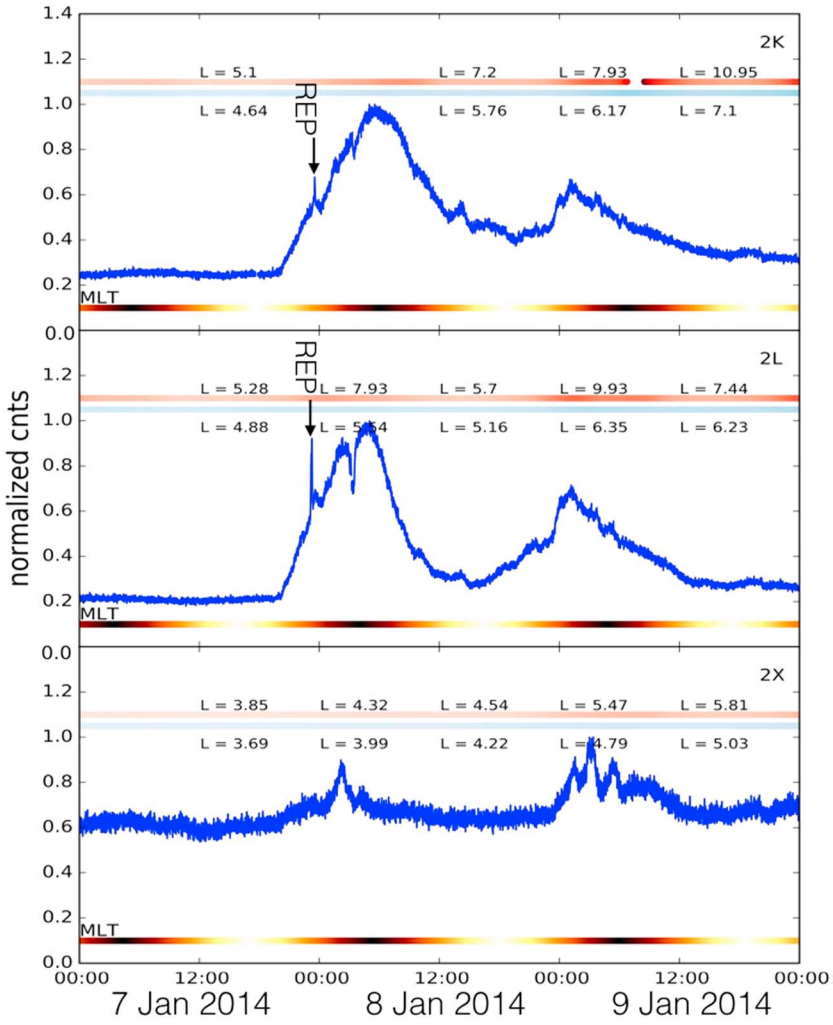

Figure 7. The normalized proton proxy for payloads 2K, 2L, and 2X. Along the top of the panels are a set of horizontal lines corresponding to the *L* value as determined by TS89 $Kp = 2$ (blue) and $Kp = 6$ (red). The horizontal line along the bottom gives the magnetic local time with white representing noon and black representing midnight. The period of contamination from a REP event observed by Payloads 2K and 2L is labeled.

Qualitatively, the increase in the proton proxy counts observed in payloads 2K, 2L, and 2X agrees with the conjugate SEP event observations by the Van Allen Probes. We use this result in the next section to explain the observations of the payloads in the outer magnetosphere in order to understand the mapping along open and closed field lines.

5. SEP and SEE Events in the Outer Magnetosphere: The Open-Closed Boundary

When we consider the payloads mapped to the outer magnetosphere and on open field lines, we find two very exciting results. The first is that BARREL was not just able to observe a SEP event but also a SEE event when on open field lines. The second result we consider with the BARREL outer payloads, using the observations of the SEP and SEE events, is one of mapping the open and closed boundary of the magnetosphere.

First, we will consider the response of the SEP event as observed at higher *L* values. Figure 8 shows the normalized proton proxy (blue) for the payloads located on field lines that mapped to either open (payload 2I) or open-closed regions (2W and 2T). The horizontal bars follow the convention set in Figure 7. The *L* values using both of the magnetic field models, TS89 with $Kp = 2$ and $Kp = 6$, are more clearly plotted in Figure 9. With such high *L* values these payloads are in regions where there should be relatively no magnetic shielding of the SEP event from the magnetosphere. In the previous section we showed that when the payloads are connected to regions of the magnetosphere where the SEP event had access, there was a corresponding

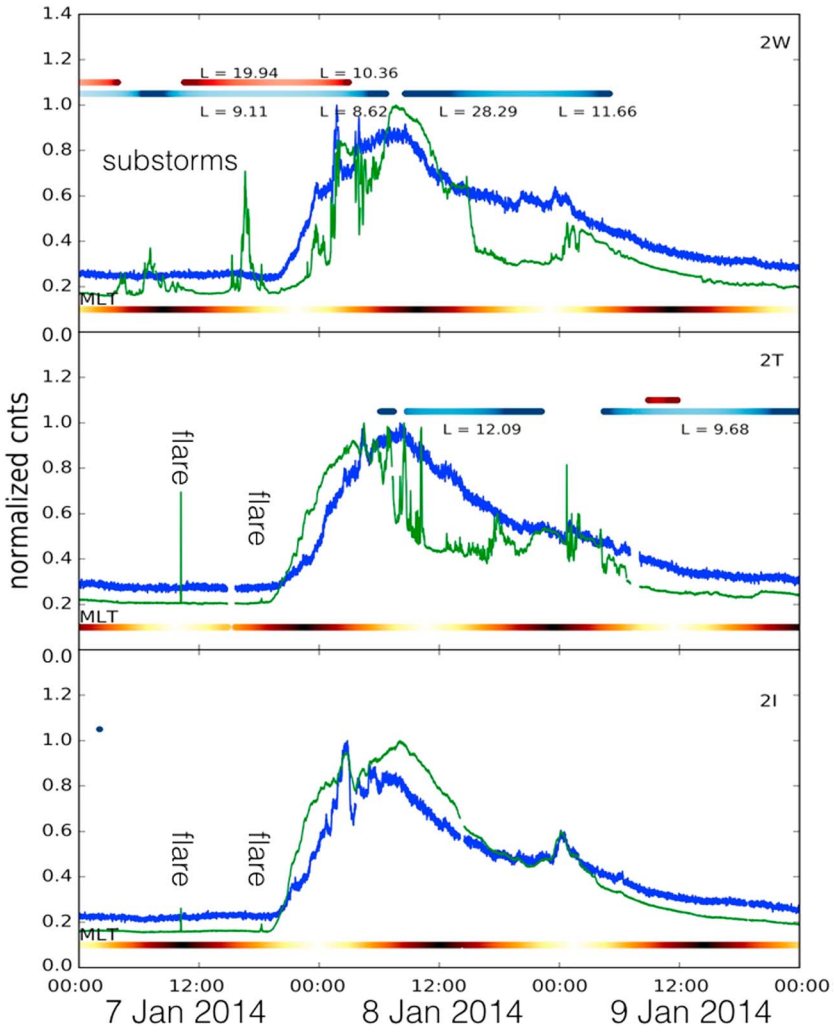

Figure 8. The normalized proton proxy (blue lines) and the normalized electron proxy (green lines) for payloads 2W, 2T, and 2I. The red (blue) straight lines show where the TS89 $Kp = 6$ (2) model maps to closed field lines. The bar on the bottom of the panels shows the local magnetic local time where black is midnight and white is noon. The periods of contamination of the electron proxy due to the solar flare X-rays and precipitation of radiation belt electrons due to substorm dynamics are labeled.

increase in the proton proxy. Here as these payloads at higher L values have less magnetic shielding or are directly connected to the solar wind, we see a smoother and more continuous response in the gamma lines. The response observed at the payloads mapping to higher L values matches most closely the response of the ~30 MeV protons observed by GOES 15 in Figure 6 (top).

There are only minor differences in the response of the SEP event between the three payloads. As payload 2W starts on field lines mapping closer to the inner magnetosphere ($L \sim 10$), the structure on the initial rise of the event is different from that observed by the other two payloads. The relative response between the three payloads in the structure observed at times does differ. For instance, the relative amplitude and oscillations observed during the rise time of the SEP event on the morning of 8 January and the peak observed near 00:00 UT on 9 January. This may be due to multiple factors including the balloons altitude and local time. A much closer look at these differences, and the energy spectra of the precipitating population, has been left to future work and the modeling efforts described in the previous sections.

The previous section focused on how the proton proxy varied with the SEP event on closed field lines where the inferred electron precipitation was dominated by loss of magnetospheric electrons (not shown here). In contrast, payload 2I is on open field lines throughout the entire event time period when mapped using both TS89 $Kp = 2$ and $Kp = 6$ magnetic field models, Figure 8 (bottom panel). By summing the energy

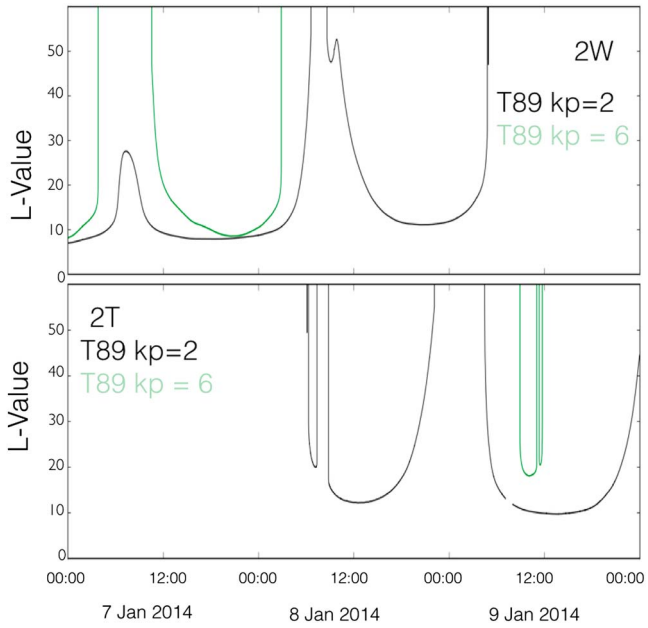

Figure 9. The *L* values which payloads 2T and 2W map to using the TS89 $Kp = 2$ (black) and $Kp = 6$ (green) input values.

channels below 500 keV (green lines in Figure 8) as defined in section 2 as the electron proxy and normalized to the maximum counts during the plotted interval, we can gain information about the precipitating electrons associated with the SEE event. As we are on field lines directly connected to the solar wind for payload 2I, the precipitating electrons are solar in origin. Effects not accounted for in this study from the precipitating protons may also be contaminating the X-ray counts below 500 keV. Future GEANT simulations of the expected proton response through the atmosphere and the payload will help quantify any expected contamination. However, if this is a large effect, we expect the structure in this new electron proxy (green line) to follow the structure of the proton proxy (blue line) in Figure 8. Although the electron and proton proxies for 2I do show some similar structures, clear differences are also observed. The rise of counts in the electron proxy is much steeper and followed by a longer but slower rise to its peak than the rise of the proton proxy. The maximum peak for the electron proxy occurs closer to noon on 8 January than the peak observed for the proton proxy. The response of both the proton and electron proxies is relatively smooth and shows a continuous decline after the peak of the events. The inferred electron response appears to recover more quickly than the protons. As the BARREL proton proxy best correlates with proton energies between approximately 15 and 50 MeV when compared to the proton responses observed in GOES Figure 6 (top), and the SEE event can be observed by ACE in Figure 6 (bottom), we can compare the relative timing between the proxies and in situ measurements. The ACE electrons and the BARREL electron proxy have a faster rise time than the observations of the protons at 10–30 MeV observed by GOES. Those same GOES protons and the BARREL proton proxy recover more slowly than the SEE event as observed by ACE as well as the BARREL electron proxy. As clear differences can be observed, the new electron proxy appears to be primarily dominated by the precipitation of electrons from the SEE event.

The SEE event can only be observed when the payloads are mapped to open field lines. The magnetosphere itself is a strong enough barrier to block these electrons from directly precipitating on closed field lines [e.g., *Kress et al.*, 2008]. As the precipitation of the SEE event is only observable on open field lines, and BARREL can distinguish between the SEE and SEP events within the polar cap, we can attempt to provide magnetic mappings of the open-closed boundary. The smooth response of the SEE event from payload 2I can act as a guide for the expected SEE event response of the other two payloads when they are also on open field lines, Figure 8. When 2W and 2T are on closed field lines, the counts in the electron proxy should decrease as the SEE event is shielded by the Earth's magnetosphere.

As shown in Figure 9, there can be a significant difference for the mapped locations of payloads 2W and 2T when using different magnetic field models. Using either TS89 $Kp = 2$ or $Kp = 6$, payloads 2W and 2T were moving across the open-closed boundary throughout the event period. Neither model matches perfectly

when the payloads are observing enhanced counts due to the SEE event as shown in Figure 8 (top and middle panel). For example, on payload 2W during the afternoon of 8 January 2014, the payload appears to have a very sudden and sustained drop in the electron proxy counts. During the early morning on 9 January 2014 the electron proxy appears to recover and look similar to payload 2I as the payload moves back onto open field lines. A similar period can be seen in both payloads 2W and 2T in the morning hours of 8 January 2014. As the payloads move between periods where they map to open and closed field lines, there appear to be large oscillations in the responses of the electron proxy. This response may be due to the payloads mapping to the magnetosheath or oscillations of the magnetopause itself. These ULF period oscillations at ~2.8 mHz are not observed in the solar wind at this time.

Typically with in situ measurements taken within the region of the radiation belts, the SEE event is shielded and not able to make it into the Earth's magnetosphere in order to be observed. When using remote sensing observations from the ground within the cusp region, it can be difficult to distinguish the SEE event signatures which can be overwhelmed by the SEP event response in the atmosphere [e.g., *Fang et al.*, 2010, 2013; *Rogers and Honary*, 2015]. As shown here, BARREL is in a unique position to be able to observe both the SEP and the SEE events simultaneously and with the same instrument.

6. Discussion/Conclusion

Although BARREL was designed with the intention to study the loss of electrons from the Earth's radiation belts, the array of balloons is also well situated to study solar energetic particle events. During the 7 January 2014 SEP event, BARREL had an array of six payloads aloft covering *L* values from the inner magnetosphere out to regions of open field lines.

The large array of floating BARREL observatories allows us to examine the earthward/geographic latitudinal extent of the SEP event. We were able to compare our results with those observed by the Van Allen Probes located in the magnetic equatorial region. We were able to show that the loss of the SEP events to the atmosphere followed the in situ observations of the SEP events by the Van Allen Probes. We are not yet able to use the BARREL data to determine the energy spectrum of the SEP events which has been left to future work. However, by comparing with the temporal and radial structures observed by the Van Allen Probes, we can infer that the majority of precipitating proton energies contributing to the creation of the gamma line features at BARREL are >15 MeV.

A SEE event with electron energies of 10s - 100s of keV as observed by ACE and inferred by BARREL was also observed on 7 January 2015 to accompany the SEP event. Although these electrons are for the most part shielded out of the magnetosphere, they can be lost to the Earth's atmosphere when they are connected to open field lines. This allows us to have an observable method for determining if the payloads are on open or closed field lines. Payload 2I was able to observe the entire SEE event as it stayed on open field lines throughout the event period. This gives a reference for the structure of the precipitating SEE event which we can then compare with the observations of payloads 2W and 2T as they move between regions of closed and open field lines. Although the magnetosphere was relatively quiet with $Kp < 4$ throughout the 3 days considered in this study, neither mapping with TS89 $Kp = 2$ or TS89 $Kp = 6$ models [*Tsyganenko*, 1989] correctly capture the open-closed boundary. This result is further complicated by structures which appear as the balloons move between these boundaries. As the balloons are relatively stationary on the time scale of hours, these relatively fast changes show how quickly this boundary can change. This behavior may be due either to the location of the magnetopause boundary itself moving or to dynamics within the magnetosheath.

Acknowledgments
The authors acknowledge NASA grants NNX15AF54G and NNX08AM58G and NSF grant AGS-1455470 and the BARREL team for use of BARREL data. The BARREL team would also like to acknowledge the National Science Foundation (NSF), the National Environmental Research Council (NERC)/British Antarctic Survey, and the South African National Antarctic Program (SANAP) for their support of the BARREL campaign. The BARREL data can be found at http://barreldata.ucsc.edu/data_products/v05/. The authors would like to thank Jeremy Faden and all of the developers of Autoplot. The REPT data were supported by RBSP-ECT funding provided by JHU/APL contract 967399 under NASA's Prime contract NAS5-01072. The authors would like to thank NOAA for the use of GOES data http://satdat.ngdc.noaa.gov/sem/goes/data/. We thank the ACE EPAM instrument team and the ACE Science Center for providing the ACE data. S. McGregor and A. Halford would like to give a special thanks to CISM for encouraging us to look at the larger "Sun to Mud" view and enabling us to form collaborations which led to this and other papers. We would like to thank BARREL team members and specifically Michael McCarthy and David Smith for their useful conversations. And last but not least, to Magritte's painting "Ceci n'est pas une pipe" for reminding us that "this" is not a subject pronoun. All other data used in this paper can be found on CDAweb.

References

Adriani, O., et al. (2015), Pamela's measurements of magnetospheric effects on high-energy solar particles, *Astrophys. J. Lett.*, *801*(1), L3.

Baker, D. N., et al. (2012), The Relativistic Electron-Proton Telescope (REPT) instrument on board the Radiation Belt Storm Probes (RBSP) spacecraft: Characterization of Earth's radiation belt high-energy particle populations, *Space Sci. Rev.*, *179*, 337–381, doi:10.1007/s11214-012-9950-9.

Bazilevskaya, G., V. Makhmutov, Y. Stozhkov, A. Svirzhevskaya, and N. Svirzhevsky (2010), Solar proton events recorded in the stratosphere during cosmic ray balloon observations in 1957–2008, *Adv. Space Res.*, *45*(5), 603–613.

Breneman, A. W., et al. (2015), Global-scale coherence modulation of radiation-belt electron loss from plasmaspheric hiss, *Nature*, *523*, 193–195.

Fang, X., C. E. Randall, D. Lummerzheim, W. Wang, G. Lu, S. C. Solomon, and R. A. Frahm (2010), Parameterization of monoenergetic electron impact ionization, *Geophys. Res. Lett.*, *37*, L22106, doi:10.1029/2010GL045406.

Fang, X., D. Lummerzheim, and C. H. Jackman (2013), Proton impact ionization and a fast calculation method, *J. Geophys. Res. Space Physics*, *118*, 5369–5378, doi:10.1002/jgra.50484.
Forbush, S. E. (1946), Three unusual cosmic-ray increases possibly due to charged particles from the Sun, *Phys. Rev.*, *70*(9–10), 771–772.
Gershman, D. J., et al. (2015), MESSENGER observations of solar energetic electrons within Mercury's magnetosphere, *J. Geophys. Res. Space Physics*, *120*, 8559–8571, doi:10.1002/2015JA021610.
Gold, R. E., S. M. Krimigis, S. E. Hawkins III, D. K. Haggerty, D. A. Lohr, E. Fiore, T. P. Armstrong, G. Holland, and L. J. Lanzerotti (1998), Electron, proton, and alpha monitor on the advanced composition explorer spacecraft, *Space Sci. Rev.*, *86*(1–4), 541–562.
Halford, A. J., et al. (2015), BARREL observations of an ICME-shock impact with the magnetosphere and the resultant radiation belt electron loss, *J. Geophys. Res. Space Physics*, *120*, 2557–2570, doi:10.1002/2014JA020873.
Kahler, S. W. (2001), Origin and properties of solar energetic particles in space, *Space Weather*, *125*, 109–122.
Klassen, A., V. Bothmer, G. Mann, M. J. Reiner, S. Krucker, A. Vourlidas, and H. Kunow (2002), Solar energetic electron events and coronal shocks, *Astron. Astrophys.*, *385*(3), 1078–1088.
Kontar, E. P., and H. A. S. Reid (2009), Onsets and spectra of impulsive solar energetic electron events observed near the Earth, *Astrophys. J.*, *695*, L140–L144.
Kozarev, K. A., R. M. Evans, N. A. Schwadron, M. A. Dayeh, M. Opher, K. E. Korreck, and B. Van der Holst (2013), Global numerical modeling of energetic proton acceleration in a coronal mass ejection traveling through the solar corona, *Astrophys. J.*, *778*(1), 43.
Kress, B. T., M. K. Hudson, M. D. Looper, J. G. Lyon, and C. C. Goodrich (2008), Global MHD test particle simulations of solar energetic electron trapping in the Earth's radiation belts, *J. Atmos. Sol. Terr. Phys.*, *70*(14), 1727–1737.
Kress, B. T., C. J. Mertens, and M. Wiltberger (2010), Solar energetic particle cutoff variations during the 29–31 October 2003 geomagnetic storm, *Space Weather*, *8*, S05001, doi:10.1029/2009SW000488.
Kühl, P., S. Banjac, N. Dresing, R. Goméz-Herrero, B. Heber, A. Klassen, and C. Terasa (2015), Proton intensity spectra during the solar energetic particle events of May 17, 2012 and January 6, 2014, *Astron. Astrophys.*, *576*, A120–A129.
LaBelle, J. (2004), High-latitude propagation studies using a meridional chain of receivers, *Ann. Geophys.*, *22*(5), 1705–1718.
Leske, R. A., R. A. Mewaldt, E. C. Stone, and T. T. von Rosenvinge (2001), Observations of geomagnetic cutoff variations during solar energetic particle events and implications for the radiation environment at the Space Station, *J. Geophys. Res.*, *106*(A12), 30,011–30,022.
Mays, M. L., et al. (2015), Propagation of the 2014 January 7 CME and resulting geomagnetic non-event, *Astrophys. J.*, *812*(2), 145.
McIlwain, C. (1966), Magnetic coordinates, *Space Sci. Rev.*, *5*, 585–598.
Mewaldt, R. A., C. M. S. Cohen, A. W. Labrador, R. A. Leske, G. M. Mason, M. I. Desai, M. D. Looper, J. E. Mazur, R. S. Selesnick, and D. K. Haggerty (2005), Proton, helium, and electron spectra during the large solar particle events of October–November 2003, *J. Geophys. Res.*, *110*, A09S18, doi:10.1029/2005JA011038.
Milan, S. E., J. S. Gosling, and B. Hubert (2012), Relationship between interplanetary parameters and the magnetopause reconnection rate quantified from observations of the expanding polar cap, *J. Geophys. Res.*, *117*, A03226, doi:10.1029/2011JA017082.
Millan, R. M., et al. (2013), The Balloon Array for RBSP Relativistic Electron Losses (BARREL), *Space Sci. Rev.*, *179*, 503–530, doi:10.1007/s11214-013-9971-z.
Miroshnichenko, L., E. Vashenyuk, and J. Pérez-Peraza (2013), Solar cosmic rays: 70 years of ground-based observations, *Geomagn. Aeron.*, *53*(5), 541–560.
Möstl, C., et al. (2015), Strong coronal channelling and interplanetary evolution of a solar storm up to Earth and Mars, *Nat. Commun.*, *6*, 7135.
Rae, I. J., K. Kabin, R. Rankin, F. R. Fenrich, W. Liu, J. A. Wanliss, A. J. Ridley, T. I. Gombosi, and D. L. De Zeeuw (2004), Comparison of photometer and global MHD determination of the open-closed field line boundary, *J. Geophys. Res.*, *109*, A01204, doi:10.1029/2003JA009968.
Reames, D. V. (1999), Particle acceleration at the Sun and in the heliosphere, *Space Sci. Rev.*, *90*(3–4), 413–491.
Rogers, N. C., and F. Honary (2015), Assimilation of real-time riometer measurements into models of 30 MHz polar cap absorption, *J. Space Weather Space Clim.*, *5*(A8), 1–18.
Savani, N., A. Vourlidas, A. Szabo, M. Mays, I. Richardson, B. Thompson, A. Pulkkinen, R. Evans, and T. Nieves-Chinchilla (2015), Predicting the magnetic vectors within coronal mass ejections arriving at Earth: 1. Initial architecture, *Space Weather*, *13*, 374–385, doi:10.1002/2015SW001171.
Share, G. H., and R. J. Murphy (2001), Atmospheric gamma rays from solar energetic particles and cosmic rays penetrating the magnetosphere, *J. Geophys. Res.*, *106*(A1), 77–92.
Singer, H., L. Matheson, and R. Grubb (1996), Monitoring space weather with the GOES magnetometers, in *Society of Photo-Optical Instrumentation Engineers (SPIE) Conference Series*, vol. 2812, edited by E. R. Washwell, pp. 229–308, Soc. of Photo-Opt. Instrum. Eng., Bellingham, Wash.
Spence, H. E., et al. (2013), Science goals and overview of the Radiation Belt Storm Probes (RBSP) Energetic Particle, Composition, and Thermal Plasma (ECT) suite on NASA's van allen probes mission, *Space Sci. Rev.*, *179*, 311, doi:10.1007/978-1-4899-7433-4_10.
Thakur, N., N. Gopalswamy, H. Xie, P. Mäkelä, S. Yashiro, S. Akiyama, and J. M. Davila (2014), Ground level enhancement in the 2014 January 6 solar energetic particle event, *Astrophys. J. Lett.*, *790*(1), L13.
Tsyganenko, N. A. (1989), A magnetospheric magnetic field model with a warped tail current sheet, *Planet. Space Sci.*, *37*(1), 5–20.
Velinov, P. I., S. Asenovski, K. Kudela, J. Lastovicka, L. Mateev, A. Mishev, and P. Tonev (2013), Impact of cosmic rays and solar energetic particles on the Earth's ionosphere and atmosphere, *J. Space Weather Space Clim.*, *3*, A14.
Woodger, L. A., A. J. Halford, R. M. Millan, M. P. McCarthy, D. M. Smith, G. S. Bowers, J. G. Sample, B. R. Anderson, and X. Liang (2015), A summary of the BARREL campaigns: Technique for studying electron precipitation, *J. Geophys. Res. Space Physics*, *120*, 4922–4935, doi:10.1002/2014JA020874.